Surface & Coatings Technology 372 (2019) 353–360

Contents lists available at ScienceDirect

Surface & Coatings Technology

journal homepage: www.elsevier.com/locate/surfcoat

In-situ creep deformation of cold-sprayed aluminum splats at elevated temperatures

Pranjal Nautiyal[a], Cheng Zhang[a], Victor Champagne[b], Benjamin Boesl[a], Arvind Agarwal[a,*]

[a] Plasma Forming Laboratory, Florida International University, 10555 West Flagler Street, Miami, FL 33174, USA
[b] U.S. Army Research Laboratory, Weapons and Materials Research Directorate, Aberdeen Proving Ground, Aberdeen, MD 20783, USA

ARTICLE INFO

Keywords:
Cold spray
High temperature creep
In situ mechanics
Splats
6061 Al alloy

ABSTRACT

This study provides new insights into temperature-dependent splat sliding mechanisms in cold-sprayed deposit by mechanical investigations at *length scales comparable to the splats*. *In-situ* indentation of 6061 Al splat structure is performed inside a scanning electron microscope from room temperature up to 400 °C. Indentation at 176 °C, which is the standard heat-treatment temperature, is characterized by enhanced nanohardness (1.65 GPa) as compared to room temperature (1.37 GPa). This is associated with the precipitate formation and improved splat-bonding due to solid-state diffusion. Further enhancement of temperature results in softening, with nanohardness ~70 MPa at 400 °C. The elastic modulus of the splat structure is ~50% of the 'bulk' modulus at room temperature and is attributed to energy-dissipation due to splat-sliding activated during indentation. 'Recovery Resistance' is computed to quantify energy-dissipation, and a five-fold jump in dissipation is noticed from room temperature to 400 °C. The elasto-plastic zone under the indenter becomes larger with temperature and comprises of multiple splats. Hence, the splat-sliding is found to be enhanced at higher temperatures. Indentation creep investigations show the transition of deformation mechanism from purely plastic (material pile-up) at lower temperatures to non-plastic (crack propagation) at 400 °C. Creep stress-exponents are computed and correspond to solute drag (~3) and dislocation creep (~4–7) mechanisms. At 400 °C, stress-concentration along the splat interfaces is observed in the vicinity of the indenter, eventually leading to crack initiation, propagation and splat delamination due to prolonged loading. These observations highlight that splat interfaces play a vital role in determining the deformation behavior of cold-sprayed materials.

1. Introduction

Cold spray is gaining increasing attention as a solid-state powder deposition process, in which powder particles are accelerated towards a substrate with supersonic velocities to obtain coatings and free-standing structures [1–3]. When the sprayed metallic particles impact upon the substrate/deposited layer, they undergo severe plastic deformation [4–6]. The bonding between the deposited splats could be mechanical interlocking or metallurgical [7–11], depending on the material and processing parameters. In the absence of strong bonding, the splats can de-bond and slide past each other upon mechanical loading. This phenomenon is called 'Splat Sliding' [12–14], which is responsible for relatively inferior elastic modulus and ductility of cold sprayed materials [15,16]. In a recent study, we experimentally demonstrated splat sliding in the cold sprayed 6061 Al by *in-situ* mechanical testing inside a scanning electron microscope [14]. It was seen that the bulk mechanical deformation is strongly influenced by splat morphology and inter-splat porosity. Coatings with significantly flattened splats are characterized by superior bonding [17], which is associated with jetting phenomenon during cold spray [18,19]. Contrary to this, coatings with limited plastic deformation during cold spray exhibited inferior splat bonding [20], which resulted in crack nucleation and rapid propagation through the coating thickness upon mechanical loading [14].

These observations indicate that the overall deformation behavior of cold sprayed materials is greatly influenced by the mechanics of splats and interfaces in the microstructure. Therefore, it is vital to probe the deformation in the *length scales comparable to the splat size* to decipher the underlying plasticity mechanisms. There are some reports on low-load nanoindentation (depths of the order of a few hundreds of nm) and mechanical mapping of individual cold-sprayed splats [16,21–23]. Splat boundaries are characterized by relatively higher hardness than splat center due to localized strain hardening. While these studies provide useful local mechanical information, they are not sufficient to understand the mechanical interactions between multiple splats. Such

* Corresponding author.
E-mail address: agarwala@fiu.edu (A. Agarwal).

https://doi.org/10.1016/j.surfcoat.2019.05.045
Received 23 March 2019; Received in revised form 14 May 2019; Accepted 15 May 2019
Available online 17 May 2019

investigation would require comparatively higher load indentation with penetration depths in the order of μm, instead of nm, so that the elasto-plastic region captures the response from splat interfaces. Temperature conditions are also expected to influence the deformation mechanisms in the splat structure. Lightweight aluminum alloys are prone to creep with a modest increase in temperatures because of their low melting points [24]. Creep is considered to be of engineering significance for temperatures exceeding $0.4T_m$ [25], which is < 100 °C for aluminum alloys. Summers et al. determined the steady-state creep rates for a bulk 6061 Al in the temperature range of 200 to 400 °C [26]. It was observed that for the material to creep at the rate of $10^{-5}\,s^{-1}$, the mechanical stresses dropped from ~220 MPa at room temperature to merely ~20 MPa at 400 °C, indicating pronounced creep at very high temperatures. Creep loading in the cold sprayed aluminum coatings can trigger de-bonding and sliding of the splats. *Currently, there is no report on high-temperature creep investigation of cold sprayed materials, which is a significant missing link in the scientific understanding of how splat structures deform at high temperatures*.

Considering the hierarchical nature of cold-sprayed microstructure, visual information about the deformation would provide deeper insights into the mechanics of splat structures. Hence, this study delves into a *real-time* examination of creep in cold-sprayed microstructure by *in-situ* indentation approach, where the deformation mechanisms in the elasto-plastic region are observed in a scanning electron microscope (SEM) [27]. These investigations are performed at elevated temperatures (up to 400 °C) to understand how the mechanical response of the splats changes as a function of temperature. The high-resolution ***real-time deformation video*** provides insight into inter-splat mechanisms activated in the elasto-plastic zone during indentation. The objective of this study is to evaluate the deformation of coatings at *microstructural length scales* for a fundamental mechanistic understanding of load-bearing by cold sprayed materials.

2. Materials and methods

2.1. Sample preparation

6061 Al coating was obtained by cold spraying gas atomized 6061 Al powder particles (Valimet CA, USA) with an average size of ~38.7 μm on a clean and polished 6061-T6 Al substrate. A high-pressure CGT 4000 cold spray system (CGT Technologies, Munich, Germany) was used, with Helium as the carrier gas. The pressure and temperature of 3.45 MPa and 384.3 °C, respectively, were maintained at the gun. The coating was then sectioned, and the exposed cross-section surface was metallographically polished for indentation investigations.

2.2. Characterization

The microstructure of the sectioned surface was examined by scanning electron microscopy (JEOL JSM-6330F field emission SEM, Tokyo, Japan). The porosity of the coating was determined by performing image analysis of multiple SEM micrographs using ImageJ software (National Institutes of Health, USA). Mechanical response of the coating was probed by *in-situ* indentation (Picoindenter, Hysitron PI 87, Bruker, Billerica, USA) at multiple temperatures: room temperature, 176 °C, 300 °C, and 400 °C. A diamond Berkovich tip (100 nm in diameter) was used. The probe, as well as the sample stage, is equipped with heaters to maintain the desired temperature during the tests. The indents were performed with 150 mN peak load. Elastic modulus and hardness values of the coating were obtained at all the test temperatures. The indentation experiments were performed inside a dual beam JEOL JIB-4500 focused ion beam/SEM system (Tokyo, Japan) for observing the deformation in real time. Time-dependent mechanical response of the coating was investigated by performing indentation creep tests. A dwell time of 200 s was programmed at the peak load during indentation to extract the creep response. At least 10 indentation experiments were performed for each condition. Thermal drift correction was conducted by a 60-s hold at the beginning of the test when the probe maintained contact with the sample with a very low pre-load (100 μN).

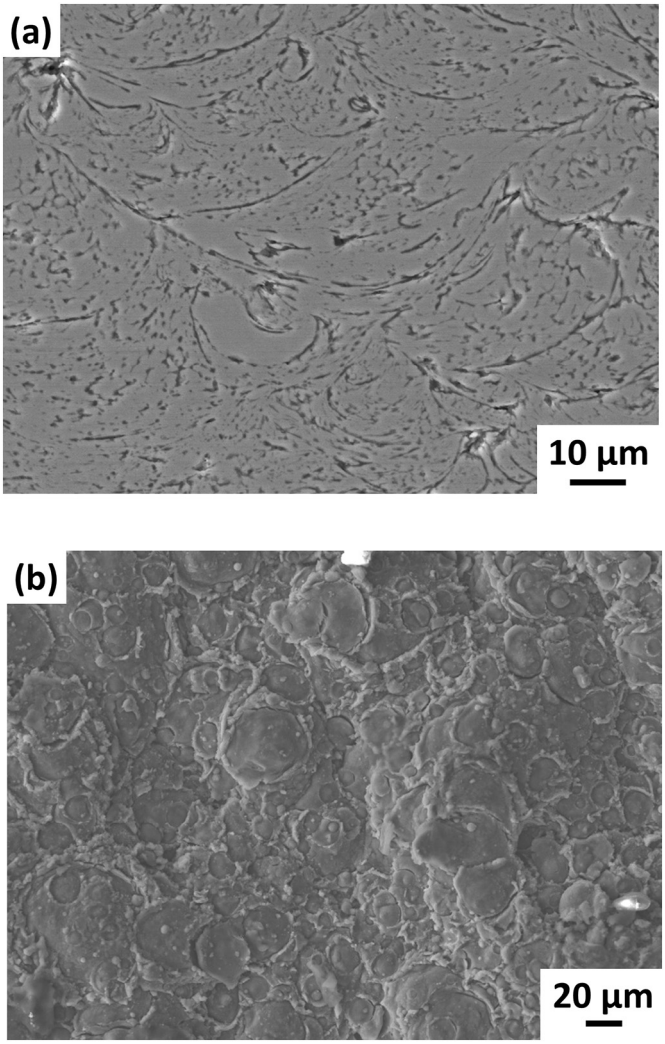

Fig. 1. SEM micrograph of cold sprayed 6061 Al deposit: (a) cross-section after polishing and etching, and (b) the top surface of the as-sprayed coating.

3. Results and discussion

3.1. Microstructure of cold sprayed 6061 Al coating

The coating microstructure is constituted by parachute-shaped splats, seen in the cross-section micrograph (Fig. 1a). The obtained coating is dense, with a very low porosity of ~0.8%. This is because of severe plastic deformation of the powder particles during cold spray. This was confirmed by the SEM micrograph of the top surface of the sprayed coating (Fig. 1b). The micrograph shows flattened splats. Because of their plastic deformability during processing, the impacting particles can easily conform to the contours of the already deposited layer, resulting in superior density. The microstructure was homogeneously dense. Therefore, the nanomechanical investigations performed in this work are not greatly influenced by porosity but reflect the response from the coating.

3.2. Localized mechanical properties at elevated temperatures

The load-displacement curves for the indentations performed at

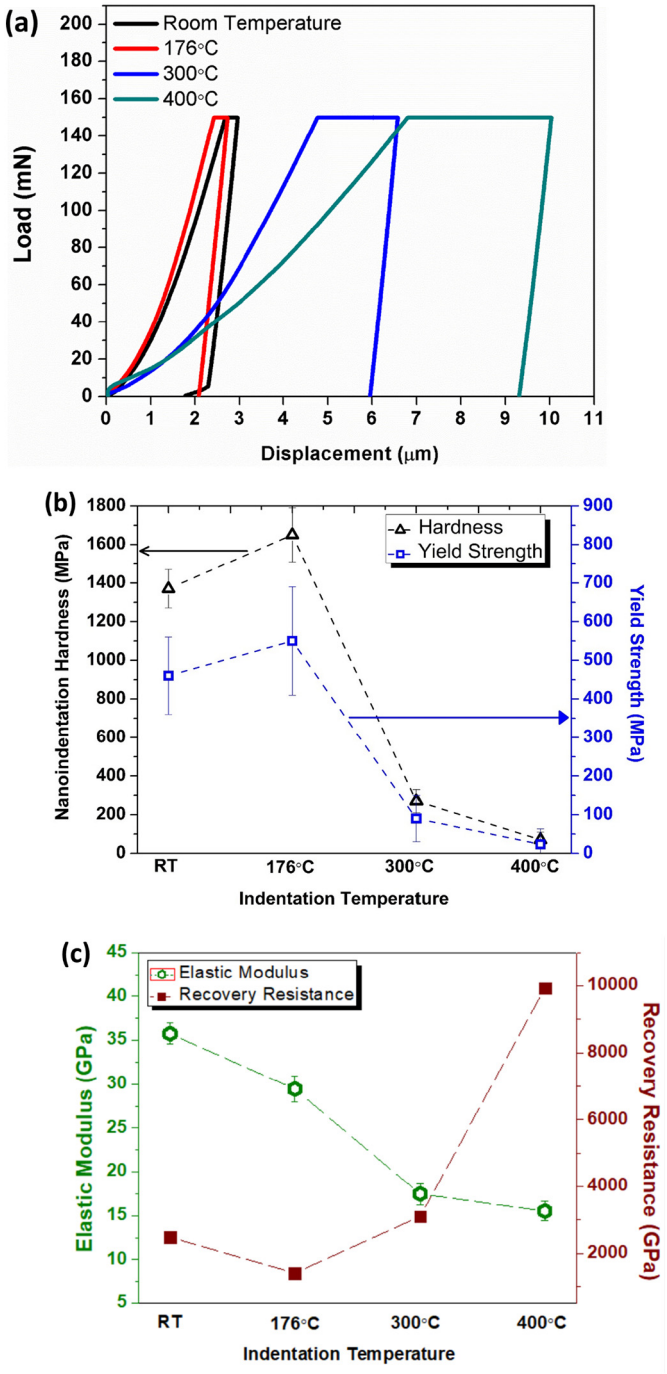

Fig. 2. (a) Comparative load-displacement curves for cold sprayed 6061 Al splat structure at room temperature, 176 °C, 300 °C and 400 °C, (b) nanohardness and yield stress values as a function of indentation temperature, and (c) elastic modulus and recovery resistance as a function of indentation temperature.

different temperatures are compared in Fig. 2a. It is seen that the resistance to deformation is slightly enhanced at 176 °C when compared with room temperature response. Further increase in temperature results in pronounced indentation deformation, with penetration depths approaching 10 μm at 400 °C which is five-fold increment as compared to the depths for room temperature indentation (~2 μm). The nanohardness values associated with the tests showed a similar trend. The splat structure in the as-sprayed coating exhibited a hardness of ~1.37 GPa at room temperature, which was enhanced to 1.65 GPa at 176 °C (shown in Fig. 2b). Thereafter, the hardness dropped dramatically to ~370 MPa at 300 °C and merely ~70 MPa at 400 °C. Multiple competing phenomena influence the plasticity mechanisms at elevated temperatures: (i) precipitate hardening due to heat-treatment, (ii) thermal diffusion-induced bonding of splats, and (iii) thermal softening due to the eradication of dislocations in the splats. It is well known that 176 °C is the standard heat treatment temperature for 6061 Al [16], responsible for the formation of strengthening precipitates (Guinier-Preston zones and Mg_2Si phases). Also, thermal exposure promotes diffusion between the splats [28], healing the inter-splat cracks and aiding in metallurgical bonding. Improved splat bonding enhances the resistance to plastic deformation, explaining the improved nanohardness. However, with further elevation of temperature, thermal softening dominates. Softening is associated with re-distribution and eradication of dislocations due to pronounced diffusion. As a result, indentation of the splats at very high temperatures leads to significant plastic flow and lower hardness.

The transition between elastic and plastic deformation is quantified by determining yield stress as a function of temperature. Indentation hardness (H) and yield stress (σ_y) are inter-related by the following equation [13]:

$$\sigma_y = H/3 \quad (1)$$

The yield stress of the splat structure at room temperature is computed to be ~460 MPa (Fig. 2b). It drops to merely ~23 MPa at 400 °C because of thermal softening. It should be noted that the room temperature yield stress of the splat structure is much higher than the reported yield stress of a 'bulk' 6061 Al substrate (< 300 MPa [16]). Relatively higher yield stress for cold sprayed microstructures is associated with significant strain hardening, as the particles can experience strains as high as 1000% during deposition [1]. Therefore, the threshold stresses required for permanent or plastic deformation of splats are higher as compared to their bulk counterparts. However, superior resistance to plastic deformation is not necessarily accompanied with higher elastic modulus. The elastic moduli of the splat structures were determined from the unloading curve, using the Oliver-Pharr technique [29]. The coating is characterized by a modulus of ~35.7 GPa at room temperature. It is noteworthy that this indentation-based elastic modulus is lower than the reported macro-scale elastic modulus (~64–68 GPa) obtained by uniaxial tensile test [30]. This difference can be attributed to the differences in the stress-state for uniaxial macro-scale *vs.* local indentation tests. The tensile stresses within the 'elastic limit' are lower and distributed throughout the sample in a macro-uniaxial test. Contrary to this, indentation loading produces high localized stresses in the microstructure. The indentation tests at room temperature in this study resulted in local tip-induced pressures exceeding 600 MPa. These stresses are concentrated around a few splats. Hence, the effect of inter-splat cracks in the microstructure on elastic modulus is prominent during local indentation, resulting in relatively lower modulus obtained by indentation. The modulus of the cold sprayed deposit drops with an increase in temperature: 29.4 GPa, 17.5 GPa, and 15.5 GPa at 176, 300 and 400 °C, respectively (Fig. 2c). It is worthy of mention that the elastic modulus of 'bulk' 6061 Al is ~70 GPa at room temperature [31]. The modulus obtained for the cold sprayed splat structure at room temperature is only ~50% of this value. The relatively inferior elastic modulus of cold sprayed coatings than their bulk counterparts is ascribed to inter-splat sliding [12–14]. The total mechanical work done during indentation has two components: (i) elastic component, which is recovered after unloading, and (ii) energy dissipated, which is not recovered. In case of cold sprayed microstructure, the inter-splat microcracks are a source of additional energy dissipation. Indentation-induced stresses can induce de-bonding and relative sliding of splats along the inter-particle boundaries. During indentation, there is a multi-axial stress-state under the indenter tip [32] (schematically shown in Fig. 3). Therefore, splat sliding can be activated along vertical as well as horizontal splat boundaries in the elasto-plastic zone (Fig. 3). This results in enhanced energy dissipation,

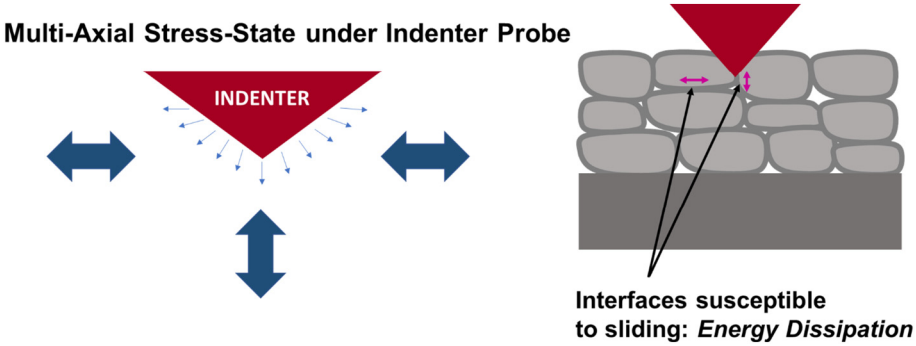

Fig. 3. Schematic representation of stress-state under an indenter probe and energy dissipation due to splat sliding.

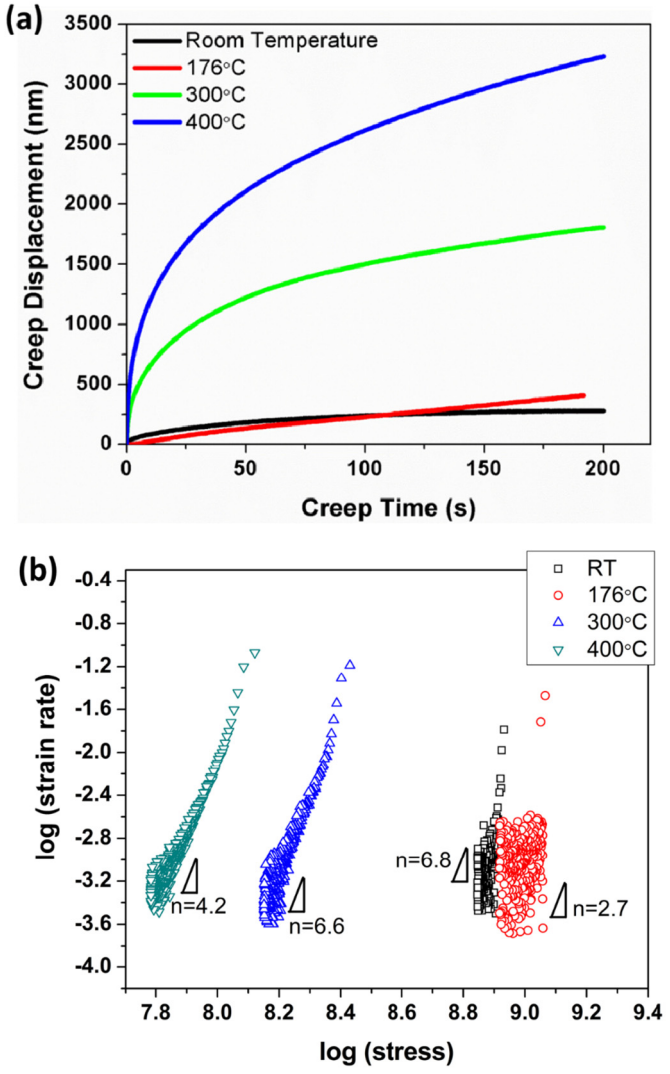

Fig. 4. Creep characteristics of cold sprayed 6061 Al deposit at room temperature, 176, 300 °C and 400 °C: (a) displacement-time plot, and (b) double logarithmic strain rate-stress plot. Creep stress exponents (slope) are appended for each temperature condition.

explaining lower modulus values than bulk 6061 Al. Bao et al. defined a *Recovery Resistance* (R_s) term to characterize energy dissipation during indentation [33]:

$$R_s = 2.263\frac{E_r^2}{H} \quad (2)$$

where E_r is reduced modulus and H is hardness. A higher value of this term indicates a larger capacity for energy dissipation. The values of R_s were computed for the indentation experiments performed at all the temperatures using Eq. (2), and are plotted in Fig. 2c. The value of R_s is lower at 176 °C, as compared to room temperature. As stated before, the formation of fine strengthening precipitates is reported when 6061 Al is heat-treated at 176 °C [16]. These precipitates constrain plastic deformation and will also likely act as 'anchors' between the splats, limiting the inter-splat sliding. Furthermore, solid-state diffusion during heat treatment heals inter-splat cracks [15]. As a result, energy dissipation is arrested. With further increase in temperature to 300 and 400 °C, the recovery resistance is much higher as compared to room temperature condition (Fig. 2c). Plastic flow is significantly enhanced at these temperatures as observed from F-h curves (Fig. 2a), explaining poor recovery or higher energy loss. These findings demonstrate that energy dissipation is an important factor that influences the elastic modulus of cold sprayed microstructures. Improving splat-splat bonding is important to restrict the dissipation of mechanical work and improve the elastic modulus/stiffness of the deposits.

Table 1
Creep stress exponents for cold sprayed 6061 Al splat structure and the corresponding mechanisms as a function of indentation temperature.

Indentation temperature	Stress exponent (n)	Governing creep mechanism
Room temperature	6.8	Power law dislocation
176 °C	2.7	Solute drag
300 °C	6.6	Power law dislocation
400 °C	4.2	Power law dislocation

3.3. High-temperature indentation creep

Creep deformation of the splat structure is investigated by programming a prolonged hold of 200 s at peak load during indentation. Dwell times during indentation-based creep tests are much smaller than conventional bulk-scale creep tests [34–36] since indentation is highly localized in nature resulting in very high stresses under the probe. The corresponding displacements as a function of time were recorded and plotted in Fig. 4a. The material exhibited a total creep displacement of ~270 nm during the hold time at room temperature. The creep deformation was higher at 176 °C, with total creep displacement recorded to be ~400 nm. With further enhancement of test temperature, creep in the cold sprayed deposit was an order of magnitude higher than room temperature creep: ~1800 nm at 300 °C and 3220 nm at 400 °C. As seen in Fig. 4a, the creep curves have two distinct regimes: an initial primary region where there is a steep increase in displacement, and a steady-state regime with a constant slope of the displacement-time curves. During creep, there are two competing processes active in the material: (i) strain hardening due to applied indentation load, and (ii) recovery, which is responsible for plastic deformation. In the steady-state regime, there is a balance between strain hardening and recovery (softening).

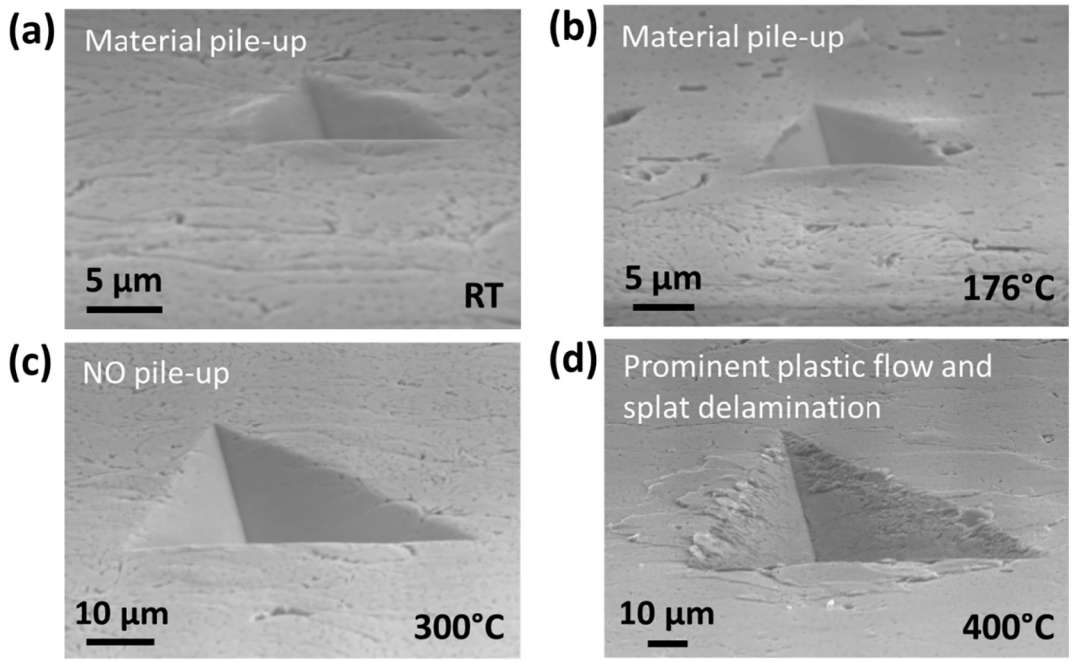

Fig. 5. SEM micrographs of indents made at: (a) room temperature, (b) 176 °C, (c) 300 °C, and (d) 400 °C.

The steady-state creep rate follows the power law equation [37]:

$$\dot{\varepsilon} = C\sigma^{n} \exp\left(-\frac{Q}{RT}\right) \tag{3}$$

where σ is indentation stress, $\dot{\varepsilon}$ is creep or strain rate, n is stress exponent, T is temperature and Q is activation energy. Stress and strain rate during indentation are computed by the following equations [36,38,39]:

$$\sigma = \frac{F}{A_p} \tag{4}$$

$$\dot{\varepsilon} = \frac{1}{h}\frac{dh}{dt} \tag{5}$$

where F is the applied load, h is the contact depth of indenter probe, and A_p is the projected area of contact, which is defined as the cross-sectional area of the indenter at a given indentation depth, h. For a Berkovich tip, which is a three-sided pyramidal indenter, A_p is expressed as:

$$A_p = 3\sqrt{3}h^2\tan^2\theta \tag{6}$$

where θ is the semi-angle and is equal to 65.27° [39].

A double logarithmic stress-strain rate relationship based on Eq. (3) is a straight line equation, with stress exponent (n) as the slope, as shown below:

$$\log\dot{\varepsilon} = \mathbf{n}\log\sigma + \log\left(C.\exp\left(-\frac{Q}{RT}\right)\right) \tag{7}$$

The stress and strain rates corresponding to the creep curves (in Fig. 4a) were computed using Eqs. (4)–(6) and plotted on a log-log scale. Fig. 4b shows the double logarithmic stress-strain rate plots for the cold sprayed deposit at all the temperature conditions. It is seen that indentation stresses are lower at elevated temperatures (300 and 400 °C) as compared to room temperature stresses. This is because of enhanced plasticity or higher penetration depths. The stresses are marginally higher at 176 °C than at room temperature, because of precipitate hardening of the alloy. The slopes of the terminal portion of these plots (steady-state region) are computed by linear fitting to obtain the stress exponents (based on Eq. (7)) [34–36]. The values of n at different indentation temperatures are marked in Fig. 4b. Stress exponent is an indicator of creep mechanisms in the material [37]. The mechanistic significance of different stress exponent values (based on prior studies in literature) is summarized in Table 1. Exponent, n is obtained to be in the range of ~3–7 in this study. These values indicate that power law dislocation and solute drag mechanisms are actively contributing towards creep in the cold sprayed 6061 Al [40–42].

3.4. Creep mechanisms in splats

The creep mechanisms were studied by SEM examination of the elasto-plastic zone comprising of splat(s) under the indenter probe. The micrographs of the indent imprints are shown in Fig. 5 for all the test temperatures. These images show visibly distinct deformation phenomena as a function of temperature. SEM micrograph at room temperature shows smaller size indent and a pile-up of material in the vicinity of the indent (Fig. 5a), suggesting that deformation zone is localized or absence of long-distance plastic flow. Arrested plasticity can be associated with work hardening during indentation. Moreover, cold sprayed splats have large dislocation density. Therefore, for creep deformation to occur, recovery by dislocation climb is likely to occur. Stress exponent of 6.8 at room temperature supports dislocation creep as the governing mechanism [41]. Pile-up of material is also seen for indentation at 176 °C (Fig. 5b). However, comparatively lower stress exponent (~2.7) is computed, suggesting dislocation creep is not the prominent mechanism. This is because dislocation climb is hindered due to the formation of strengthening precipitates in the splats. Exponent value close to 3 is associated with solute drag, caused by diffusion of solute atoms around moving dislocations [42]. The concentration gradient is created in the splats due to precipitation, which will enhance diffusion, thereby favoring creep by solute drag [43].

In contrast to the deformation at room temperature and 176 °C, indent made at 300 °C does not exhibit any material pile-up and has significantly larger size (Fig. 5c). At elevated temperatures, coarsening or growth of dislocations takes place. This will lead to lower dislocation density in the splats, leading to recovery. Coarser dislocation network is associated with lower flow stress (σ_f), which can be understood by the following relation [44]:

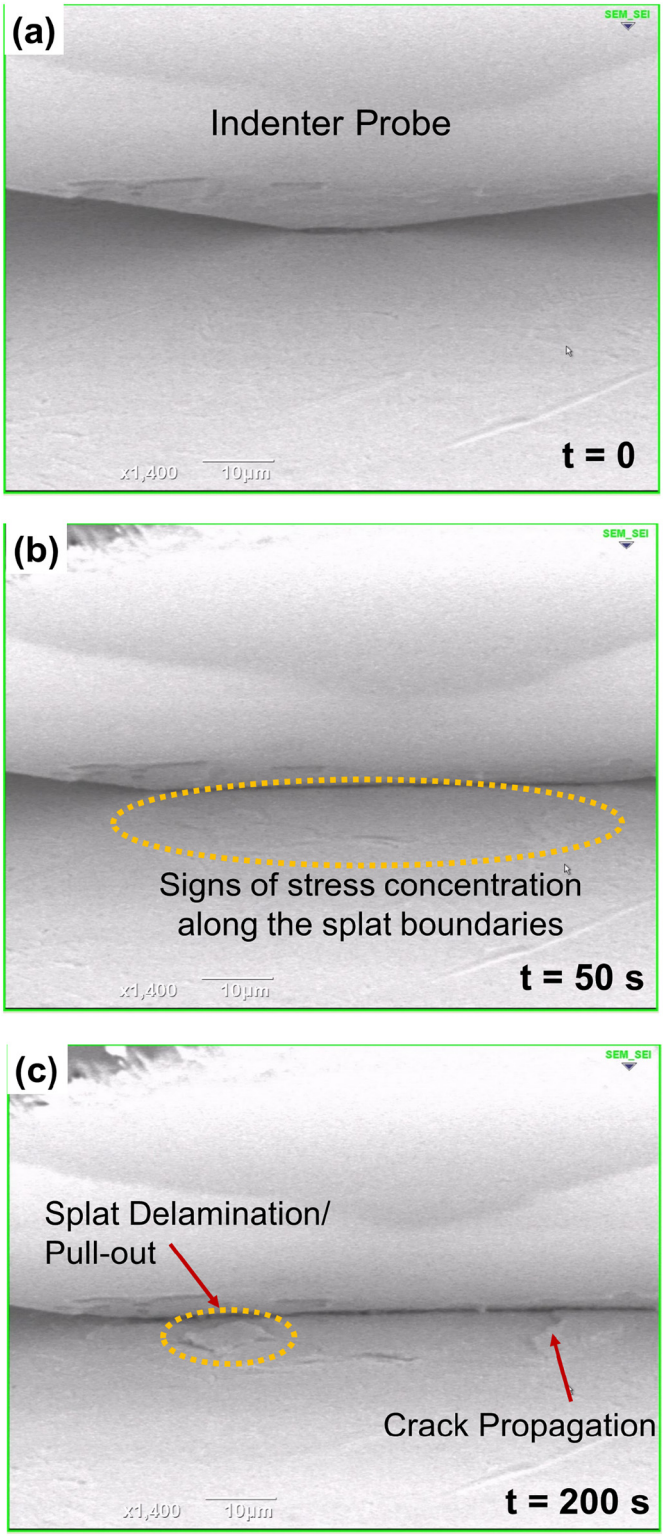

Fig. 6. Progression of indentation creep test at 400 °C captured in real time inside an electron microscope: (a) beginning of the creep test ($t = 0$), (b) at $t = 50$ s showing the appearance of splat boundaries near the indenter probe, indicating stress concentration, and (c) crack propagation and splat delamination phenomena at the end of creep test.

$$<\lambda> = \frac{\alpha \mu b}{\sigma_f} \quad (8)$$

where $<\lambda>$ is the mean mesh size of dislocation network, α is a constant, μ is the shear modulus, and b is Burgers vector. Mesh size and flow stress are inversely related, which explains enhanced plasticity (large indent size) due to coarsening of dislocations at elevated temperatures. Stress exponent is computed to be 6.6, which is indicative of dislocation creep mechanism.

At 400 °C, plastic flow is significantly enhanced. The SEM micrograph in Fig. 5d shows delamination and detachment of splats. Dislocation climb is energetically favored at high temperatures, resulting in pronounced recovery. Softening of splat structure due to recovery is evidenced by the low nanohardness value of ~70 MPa at 400 °C. Stress exponent is found to be 4.2, which is associated with recovery due to dislocation climb [37]. *In situ* indentation at 400 °C showed the activation of non-plastic deformation mechanisms (Supplementary Video V1). The SEM snapshots of the progression of indentation are shown in Fig. 6. While the initial deformation is a plastic flow of material, further loading leads to crack initiation and propagation along the splat boundaries. As the creep loading continues, there is delamination, detachment, and pull-out of the splats. The observed embrittlement can be explained by solute segregation in the cold sprayed microstructure. Rokni et al. observed enhanced segregation of Si, Cu, Mg and Fe-rich precipitates at the grain boundaries in 6061 Al after cold spray, when compared with pre-spray powder particles [45]. This accentuated solute segregation is attributed to the defects introduced in the microstructure during cold spray, which tend to migrate towards boundary sinks.

This dramatic transition in deformation mechanisms can be understood in terms of the deformation zone under the indenter. In previous reports, it has been shown that heat-treatment leads to healing of inter-splat cracks [14,28]. As a result, the dislocation movement between the splats is favorable, and the deformation is not localized to a single splat. This results in the much larger elasto-plastic region, encompassing multiple splats (schematically shown in Fig. 7). From the SEM micrographs (Figs. 5d and 6), the edge length of the indent imprint at 400 °C is around ~80 μm, whereas the average diameter of a single splat is ~30 μm. Consequently, deformation behavior is not only governed by single splat mechanics, but also by the splat interfaces. Splat boundaries act as discontinuities in the cold sprayed microstructure, and hence, these interfaces are susceptible to excessive stress concentration upon indentation loading (as seen in the SEM micrograph in Fig. 6b). In addition to indenter-induced stresses, the interfaces also experience stresses due to thermal expansion of individual splats at elevated temperatures. This leads to crack initiation at the stressed interfaces. Once initiated, the cracks tend to propagate along the splat boundaries (Fig. 6c). Gavras and co-workers also observed that particle (splat) boundaries in the microstructure play a critical role in determining crack advancement during fatigue loading of 6061Al (specially for high driving forces) [30]. These findings of this study strongly suggest that splat sliding is a critical variable that determines the time-dependent creep behavior of cold-sprayed coatings and free-standing structures.

4. Conclusion

In this study, creep response of cold sprayed 6061 Al splat structure is probed by *in situ* indentation inside an SEM from room temperature to 400 °C. The deformation mechanisms are observed in real time. The major conclusions are as follows:

- Nanohardness at 176 °C (1.65 GPa) improves as compared to room temperature (1.37 GPa) due to enhanced splat-bonding caused by solid-state diffusion. Further increase in temperature results in softening as the hardness drops to merely ~70 MPa at 400 °C. Enhanced plasticity is associated with eradication and re-distribution of dislocations in the splats.
- The elastic modulus of the splat structure is ~50% the modulus of 'bulk' 6061 Al at room temperature. Indentation-induced stresses activate splat-sliding in the cold sprayed microstructures, responsible for energy dissipation and consequently lower elastic

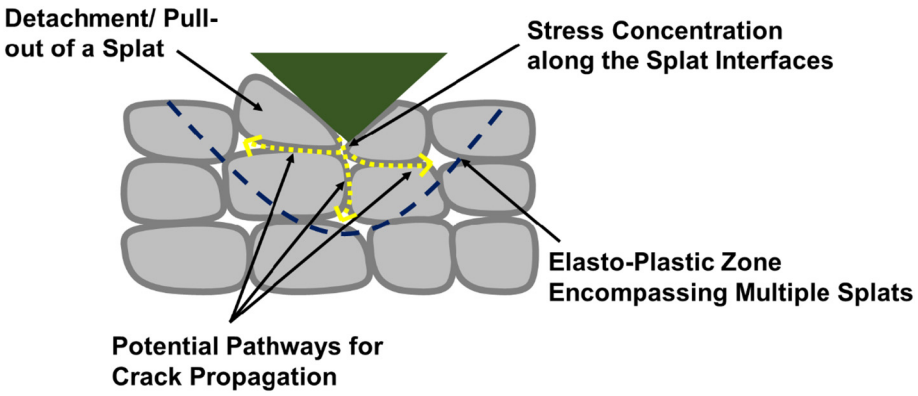

Fig. 7. Schematic representation of indentation-induced crack initiation, propagation and splat delamination mechanisms in the elasto-plastic region under indenter probe.

modulus. Splat sliding is quantified by computing recovery resistance. Larger elasto-plastic zone, encompassing multiple splats under the indenter at higher temperatures is responsible for accentuated splat sliding. Five-fold enhancement in recovery resistance is observed at 400 °C as compared to room temperature.

- Creep investigations reveal a transition in deformation characteristics from predominantly plastic (material pile-up) at lower temperatures to the activation of crack initiation and propagation at 400 °C. Stress-exponent calculations indicate solute drag (n~3) and dislocation creep (n~4–7) mechanisms. *In-situ* SEM video shows stress-concentration along the splat boundaries during indentation creep, eventually leading to crack initiation, propagation and splat delamination.

The findings of this study highlight the importance of splat bonding and splat sliding in the mechanical performance of cold sprayed materials. It is vital to map cold spray processing conditions with inter-splat bonding to engineer materials with predictable mechanical properties.

Supplementary data to this article can be found online at https://doi.org/10.1016/j.surfcoat.2019.05.045.

Acknowledgments

The authors acknowledge the Army Research Laboratory for Grant W911NF15-2-0026 (Subaward No. 504108-78052). The authors also thank Dr. C. A. Widener (South Dakota School of Mines & Technology, USA) for providing the cold sprayed coatings used in this study. BB acknowledges the Office of Naval Research DURIP grant (N00014-16-1-2604) for establishing *in-situ* nanoindenter facility at FIU. PN thanks Florida International University (FIU) Graduate School for the financial support through Presidential Fellowship award. The authors thank Xiaolong Lu (FIU) for assisting with sample preparation to perform indentation tests. Advanced Materials Engineering Research Institute (AMERI) at FIU is acknowledged for the research facilities used in this study.

References

[1] H. Assadi, H. Kreye, F. Gärtner, T. Klasen, Cold spraying – a materials perspective, Acta Mater. 116 (2016) 382–407, https://doi.org/10.1016/j.actamat.2016.06.034.
[2] V.K. Champagne, The Cold Spray Materials Deposition Process: Fundamentals and Applications, CRC Press, Boca Raton, 2007.
[3] T. Schmidt, F. Gärtner, H. Assadi, H. Kreye, Development of a generalized parameter window for cold spray deposition, Acta Mater. 54 (2006) 729–742, https://doi.org/10.1016/j.actamat.2005.10.005.
[4] H. Assadi, F. Gärtner, T. Stoltenhoff, H. Kreye, Bonding mechanism in cold gas spraying, Acta Mater. 51 (2003) 4379–4394, https://doi.org/10.1016/S1359-6454(03)00274-X.
[5] M.H.- Gangaraj, D. Veysset, K.A. Nelson, C.A. Schuh, In-situ observations of single micro-particle impact bonding, Scr. Mater. 145 (2018) 9–13, https://doi.org/10.1016/j.scriptamat.2017.09.042.
[6] K. Balani, A. Agarwal, S. Seal, J. Karthikeyan, Transmission electron microscopy of cold sprayed 1100 aluminum coating, Scr. Mater. 53 (2005) 845–850, https://doi.org/10.1016/j.scriptamat.2005.06.008.
[7] Y. Xie, S. Yin, C. Chen, M.-P. Planche, H. Liao, R. Lupoi, New insights into the coating/substrate interfacial bonding mechanism in cold spray, Scr. Mater. 125 (2016) 1–4, https://doi.org/10.1016/j.scriptamat.2016.07.024.
[8] C. Borchers, F. Gärtner, T. Stoltenhoff, H. Kreye, Microstructural bonding features of cold sprayed face centered cubic metals, J. Appl. Phys. 96 (2004) 4288–4292, https://doi.org/10.1063/1.1789278.
[9] G. Bae, S. Kumar, S. Yoon, K. Kang, H. Na, H.-J. Kim, C. Lee, Bonding features and associated mechanisms in kinetic sprayed titanium coatings, Acta Mater. 57 (2009) 5654–5666, https://doi.org/10.1016/j.actamat.2009.07.061.
[10] S. Kumar, M. Ramakrishna, N.M. Chavan, S.V. Joshi, Correlation of splat state with deposition characteristics of cold sprayed niobium coatings, Acta Mater. 130 (2017) 177–195, https://doi.org/10.1016/j.actamat.2017.03.023.
[11] M.R. Rokni, C.A. Widener, V.R. Champagne, Microstructural evolution of 6061 aluminum gas-atomized powder and high-pressure cold-sprayed deposition, J. Therm. Spray Technol. 23 (2014) 514–524, https://doi.org/10.1007/s11666-013-0049-y.
[12] F. Tang, J.M. Schoenung, Evolution of Young's modulus of air plasma sprayed yttria-stabilized zirconia in thermally cycled thermal barrier coatings, Scr. Mater. 54 (2006) 1587–1592, https://doi.org/10.1016/j.scriptamat.2006.01.021.
[13] Y. Chen, S.R. Bakshi, A. Agarwal, Intersplat friction force and splat sliding in a plasma-sprayed aluminum alloy coating during nanoindentation and micro-indentation, ACS Appl. Mater. Interf. 1 (2009) 235–238, https://doi.org/10.1021/am800114h.
[14] P. Nautiyal, C. Zhang, V.K. Champagne, B. Boesl, A. Agarwal, *In-situ* mechanical investigation of the deformation of splat interfaces in cold-sprayed aluminum alloy, Mater. Sci. Eng. A 737 (2018) 297–309, https://doi.org/10.1016/j.msea.2018.09.065.
[15] G. Sundararajan, N.M. Chavan, S. Kumar, The elastic modulus of cold spray coatings: influence of inter-splat boundary cracking, J. Therm. Spray Technol. 22 (2013) 1348–1357, https://doi.org/10.1007/s11666-013-0034-5.
[16] M.R. Rokni, C.A. Widener, O.C. Ozdemir, G.A. Crawford, Microstructure and mechanical properties of cold sprayed 6061 Al in as-sprayed and heat treated condition, Surf. Coat. Technol. 309 (2017) 641–650, https://doi.org/10.1016/j.surfcoat.2016.12.035.
[17] G. Bae, J.-il Jang, C. Lee, Correlation of particle impact conditions with bonding, nanocrystal formation and mechanical properties in kinetic sprayed nickel, Acta Mater. 60 (2012) 3524–3535, https://doi.org/10.1016/j.actamat.2012.03.001.
[18] M.H.- Gangaraj, D. Veysset, V.K. Champagne, K.A. Nelson, C.A. Schuh, Adiabatic shear instability is not necessary for adhesion in cold spray, Acta Mater. 158 (2018) 430–439, https://doi.org/10.1016/j.actamat.2018.07.065.
[19] P.C. King, S.H. Zahiri, M. Jahedi, Focused ion beam micro-dissection of cold-sprayed particles, Acta Mater. 56 (2008) 5617–5626, https://doi.org/10.1016/j.actamat.2008.07.034.
[20] G. Bae, Y. Xiong, S. Kumar, K. Kang, C. Lee, General aspects of interface bonding in kinetic sprayed coatings, Acta Mater. 56 (2008) 4858–4868, https://doi.org/10.1016/j.actamat.2008.06.003.
[21] Y. Zou, D. Goldbaum, J.A. Szpunar, S. Yue, Microstructure and nanohardness of cold-sprayed coatings: Electron backscattered diffraction and nanoindentation studies, Scr. Mater. 62 (2010) 395–398, https://doi.org/10.1016/j.scriptamat.2009.11.034.
[22] M.R. Rokni, C.A. Widener, G.A. Crawford, M.K. West, An investigation into microstructure and mechanical properties of cold sprayed 7075 Al deposition, Mater. Sci. Eng. A 625 (2015) 19–27, https://doi.org/10.1016/j.msea.2014.11.059.
[23] D. Goldbaum, R.R. Chromik, S. Yue, E. Irissou, J.-G. Legoux, Mechanical property mapping of cold sprayed Ti splats and coatings, J. Therm. Spray Technol. 486 (2011) 486–496, https://doi.org/10.1007/s11666-010-9546-4.
[24] P.S. Phani, W.C. Oliver, A direct comparison of high-temperature nanoindentation creep and uniaxial creep measurements for commercial purity aluminum, Acta Mater. 111 (2016) 31–38, https://doi.org/10.1016/j.actamat.2016.03.032.

[25] W.D. Callister, Materials Science & Engineering, John Wiley & Sons, New York, 2007.
[26] P.T. Summers, Y. Chen, C.M. Rippe, B. Allen, A.P. Moritz, S.W. Case, B.Y. Lattimer, Overview of aluminum alloy mechanical properties during and after fires, Fire Sci. Rev. 4 (2015) 3, https://doi.org/10.1186/s40038-015-0007-5.
[27] P. Nautiyal, M. Mujawar, B. Boesl, A. Agarwal, *In-situ* mechanics of 3D graphene foam based ultra-stiff and flexible metallic metamaterial, Carbon 137 (2018) 502–510, https://doi.org/10.1016/j.carbon.2018.05.063.
[28] P.S. Phani, V. Vishnukanthan, G. Sundararajan, Effect of heat treatment on properties of cold sprayed nanocrystalline copper alumina coatings, Acta Mater. 55 (2007) 4741–4751, https://doi.org/10.1016/j.actamat.2007.04.044.
[29] W.C. Oliver, G.M. Pharr, An improved technique for determining hardness and elastic modulus using load and displacement sensing indentation experiments, J. Mater. Res. 7 (1992) 1564–1583, https://doi.org/10.1557/JMR.1992.1564.
[30] A.G. Gavras, D.A. Lados, V.K. Champagne, R.J. Warren, Effects of processing on microstructure evolution and fatigue crack growth mechanisms in cold-spray 6061 aluminum alloy, Int. J. Fatigue 110 (2018) 49–62, https://doi.org/10.1016/j.ijfatigue.2018.01.006.
[31] J.G. Kaufman, Properties of Aluminum Alloys: Tensile, Creep, and Fatigue Data at High and Low Temperatures, The Aluminum Association and ASM International, Materials Park, 1999.
[32] J,.-H. Shin, S.-H. Kim, T.K. Ha, K.H. Oh, I.-S. Choi, H.N. Han, Nanoindentation study for deformation twinning of magnesium single crystal, Scr. Mater. 68 (2013) 483–486, https://doi.org/10.1016/j.scriptamat.2012.11.030.
[33] Y.W. Bao, W. Wang, Y.C. Zhou, Investigation of the relationship between elastic modulus and hardness based on depth-sensing indentation measurements, Acta Mater. 52 (2004) 5397–5404, https://doi.org/10.1016/j.actamat.2004.08.002.
[34] P. Nautiyal, J. Jain, A. Agarwal, A comparative study of indentation induced creep in pure magnesium and AZ61 alloy, Mater. Sci. Eng. A 630 (2015) 131–138, https://doi.org/10.1016/j.msea.2015.01.075.
[35] P. Nautiyal, J. Jain, A. Agarwal, Influence of loading path and precipitates on indentation creep behavior of mg-6 wt.%Al-1 wt.%Zn, Mater. Sci. Eng. A 650 (2016) 183–189, https://doi.org/10.1016/j.msea.2015.10.040.
[36] R. Goodall, T.W. Clyne, A critical appraisal of the extraction of creep parameters from nanoindentation data obtained at room temperature, Acta Mater. 54 (2006) 5489–5499, https://doi.org/10.1016/j.actamat.2006.07.020.
[37] H. Oikawa, S. Karashima, On the stress exponent and the rate-controlling mechanism of high-temperature creep in some solid solutions, Metall. Trans. 5 (1974) 1179–1182, https://doi.org/10.1007/BF02644330.
[38] M.J. Mayo, W.D. Nix, A micro-indentation study of superplasticity in Pb, Sn, and Sn–38 wt.% Pb, Acta Metall. 36 (1988) 2183–2192, https://doi.org/10.1016/0001-6160(88)90319-7.
[39] A.C. Fischer-Cripps, Nanoindentation, Springer, New York, 2002.
[40] G. Graiss, A.F.A. El-Rehim, Examination of breakdown stress in creep by viscous glide in Al–5?5 at.-%Mg solid solution alloy at high-stress levels, Mater. Sci. Technol. 23 (2007) 1144–1148, https://doi.org/10.1179/174328407X226545.
[41] I.C. Hsiao, J.C. Huang, Deformation mechanisms during low- and high-temperature superplasticity in 5083 Al-Mg alloy, Metall. Mater. Trans. A 33A (2002) 1373–1384, https://doi.org/10.1007/s11661-002-0062-0.
[42] F. Zhang, W.A. Curtin, Atomistically informed solute drag in Al–Mg, Modelling Simul. Mater. Si. Eng. 16 (2008) 055006, , https://doi.org/10.1088/0965-0393/16/5/055006.
[43] M.R. Rokni, C.A. Widener, S.P. Ahrenkiel, B.K. Jasthi, V.R. Champagne, Annealing behaviour of 6061 aluminium deposited by high pressure cold spray, Surf. Eng. 30 (2014) 361–368, https://doi.org/10.1179/1743294413Y.0000000209.
[44] L. Shi, D.O. Northwood, Dislocation network models for recovery creep deformation, J. Mater. Sci. 28 (1993) 5963–5974, https://doi.org/10.1007/BF00365006.
[45] M.R. Rokni, C.A. Widener, V.R. Champagne, Microstructural stability of ultrafine grained cold sprayed 6061 aluminum alloy, Appl. Surf. Sci. 290 (2014) 482–489, https://doi.org/10.1016/j.apsusc.2013.11.127.